LANGMUIR Article
Cite This: Langmuir 2019, 35, 5911−5920 pubs.acs.org/Langmuir

Molecular Driving Forces in Peptide Adsorption to Metal Oxide Surfaces

Coco M. Mao,[†] Janani Sampath,[‡] K. G. Sprenger,[‡] Gary Drobny,[§] and Jim Pfaendtner*[,‡]

[†]Department of Materials Science and Engineering, [‡]Department of Chemical Engineering, and [§]Department of Chemistry, University of Washington, Seattle, Washington 98195, United States

Supporting Information

ABSTRACT: Molecular recognition between peptides and metal oxide surfaces is a fundamental process in biomineralization, self-assembly, and biocompatibility. Yet, the underlying driving forces and dominant mechanisms remain unclear, bringing obstacles to understand and control this process. To elucidate the mechanism of peptide/surface recognition, specifically the role of serine phosphorylation, we employed molecular dynamics simulation and metadynamics-enhanced sampling to study five artificial peptides, DDD, DSS, DpSpS, DpSpSGKK, and DpSKGpSK, interacting with two surfaces: rutile TiO_2 and quartz SiO_2. On both surfaces, we observe that phosphorylation increases the binding energy. However, the interfacial peptide conformation reveals a distinct binding mechanism on each surface. We also study the impact of peptide sequence to binding free energy and interfacial conformation on both surfaces, specifically the impact on the behavior of phosphorylated serine. Finally, the results are discussed in context of prior studies investigating the role of serine phosphorylation in peptide binding to silica.

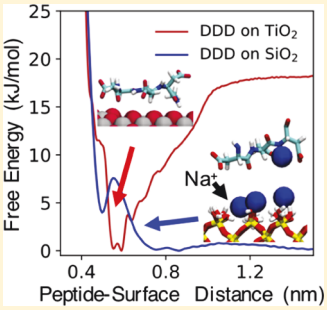

INTRODUCTION

Molecular recognition between peptides and surfaces plays an important role in many biological systems and processes. It is the underlying mechanism of a wide range of practical applications such as drug delivery,[1,2] biosensor design,[3,4] biomineralization,[5,6] materials selectivity and self-assembly/formation,[7,8] and processes or applications that face challenges of toxicity and/or biocompatibility.[9−14] Though the fundamentals of molecular recognition processes remain largely unclear, the composition and sequencing of amino acids are known to play important roles in regulating peptide/surface affinity. Additionally, the presence of posttranslational modifications (PTMs) such as phosphorylation or methylation of peptide residues could have dramatic effects on peptide conformation and could lead to a more complex interfacial system.[15−17] Identifying amino acids that are active participants in peptide/surface binding is one of the first steps in understanding peptide adsorption and is therefore a prerequisite for rational peptide design in surface-based applications. However, isolating the effects of specific amino acids, whether naturally occurring or altered through PTMs, or the combined effects of groups of amino acids (i.e., "binding sites"), is nontrivial. This remains a significant challenge that limits our understanding of peptide/surface interactions and molecular recognition processes.

With the development of technologies that can synthesize peptide sequences with precision, artificial peptides can now be rationally designed to isolate the effects of specific amino acid sequences on peptide/surface adsorption.[17−19] To date, many artificial peptides have been designed for this purpose and studied through both experiments and simulations, with simplified sequences and short lengths in the form of homopeptides, interdigitated peptides, and modified naturally occurring or synthetically designed peptides. For example, Walsh et al. recently employed molecular dynamics (MD) simulations to calculate and compare the binding energies of three trihomopeptides (YYY, HHH, and SSS) on a gold surface.[20] Carravetta and Monti have designed two dipeptides, Ala−Glu and Ala−Lys, to represent two extremities of self-assembly peptide EAK16-II and simulated their interaction with the TiO_2(110) surface.[21] Latour et al.[22] have designed eight different zwitterionic peptides interacting with nine different functionalized alkanethiol self-assembled monolayer surfaces to verify the adsorption energy calculated by the CHARMM force field and biased-energy replica exchange. This work is reproduced by Wei and Knotts[23] with a coarse-grained model and also agrees with experimental measurements on adsorption energy.[24] Tan et al. experimentally measured the binding affinity of tryptophan- and histidine-interdigitated peptides (XWXWXWX and XHXHXHX, respectively, where X is any desired neighboring amino acid) with gold particles.[25] Similarly, gold-binding peptides were designed by Hnilova et al. in both cyclic and linear form to investigate the effects of architectural constraints on binding to gold through both experiments and computational modeling.[26]

Even with designed sequences of relatively few amino acids, the chemistry of the surface (e.g., complex nanoscale patterning of positive and negative surface charges) can

Received: April 27, 2018
Revised: March 28, 2019
Published: April 8, 2019

DOI: 10.1021/acs.langmuir.8b01392
Langmuir 2019, 35, 5911−5920

significantly complicate our understanding of peptide/surface interactions. The above examples all featured adsorption to gold, a relatively simple surface. Metal oxide surfaces that have more complex surface chemistries, such as titanium or silicon dioxide (TiO_2 or SiO_2, respectively), have garnered a great deal of attention in recent years because of their promising biocompatible properties.[27−32] While much remain unknown about the mechanisms of biomolecular adsorption to these types of surfaces, some progress has been made through the combined efforts of experimental and computational studies. Experimentally, atomic force microscopy has been used to study the binding of Ti-recognizing peptide RKLPDA and one of its mutants to TiO_2, providing information about the relative peptide/surface interaction strengths of the two systems.[33] Peptides have also been rationally designed to promote titania formation,[34] and adsorption to TiO_2 surfaces has been used to enrich protein phosphorylation by taking advantage of the selectivity of phosphorylated residues.[35] More recently, Puddu and co-workers investigated the titania nanoparticle-forming capabilities of two peptides with high affinity for titania, gaining insight into key peptide/surface interactions governing titania mineralization across a range of different solution conditions.[6]

Arguably, more data are currently available on biomolecular adsorption to SiO_2 surfaces, compared to TiO_2 surfaces. For instance, Vertegel et al. studied the effect of silica nanoparticle sizes on the adsorption behavior and interfacial structure of chicken egg lysozyme with adsorption isotherms, activity assays, and circular dichroism spectroscopy.[36] Puddu and Perry recently used fluorimetric assays to quantify the impact of pH on the binding behavior of charged peptides on amorphous silica nanoparticles.[37] Additionally, by using a variety of experimental techniques in addition to MD simulations, the dual mechanisms of ion pairing and hydrogen bond formation between peptides and silica surfaces have been studied in detail.[38]

These examples demonstrate the use of molecular simulations in addition to experiments to breakdown and understand the complexities of biomolecular adsorption to metal oxide surfaces. In all these studies, MD simulations provided fundamental support for the proposed silica binding mechanism through strong agreement of peptide/silica adsorption energies calculated via simulations and experiments and by quantifying the contributions of individual surface-bound amino acids to the overall binding strength of the peptides.[38] It also points, however, to the necessity of using an accurate and realistic surface model (in addition to the solute model) to provide meaningful physical insights. In this regard, the force field built by Matsui and Akaogi (MA)[39] is the most well-known model for bulk rutile TiO_2. It has proved to be successful in many simulations of both bulk and interfacial TiO_2,[40−46] and many modifications have been made to this model:[47−50] Machesky et al. built multiple models of the TiO_2(110) surface with different hydroxylation and charges,[47] and Köppen and Langel[51] have derived Lennard-Jones (LJ)[52] parameters from the Buckingham potential used in the original MA force field for better agreement with force fields that are designed for organic molecules, such as Amber[53] and CHARMM,[54] and used this to simulate the adsorption of peptides on (100) TiO_2. Similar work has been done by Brandt and Lyubartsev,[49] where they optimized the LJ form force field to obtain a water−TiO_2 enthalpy close to experimental data. Unlike titania, where most studies focus on crystal structures, more computational models are available to simulate silica in both crystalline and amorphous forms.[55] Emami et al. have developed a silica surface model database that covers a wide range of silica surface chemistry and pH.[56]

Enhanced sampling techniques have also been applied to metal oxide-based systems to overcome strong biomolecule/surface binding forces that can hinder sampling in classical MD simulations.[27,57,58] For example, Walsh et al. predicted adsorption free energies of amino acid analogues on a negatively charged (110) surface of rutile TiO_2 using metadynamics.[32] Brandt and Lyubartsev calculated adsorption profiles of side-chain analogues of the 20 naturally occurring amino acids as well as a titanium-binding peptide on the (100) surface of TiO_2 using both metadynamics and umbrella sampling.[50] Related to the present work, the binding of silaffin peptide R5 to silica and the role of phosphorylation were previously considered with MD[16] as well as the role of R5 in templating the growth of freestanding silica sheets.[59]

Here, we build on the progress of these past studies using simple, rationally designed peptide sequences to investigate the molecular driving forces behind peptide adsorption to inorganic, metal oxide surfaces. We focus on elucidating the effects of posttranslational phosphorylation and peptide sequence on the surface-bound conformations and binding energies of peptides adsorbed to metal oxide surfaces and quantify whether the location, order, and extent of phosphorylation serve to increase or decrease the binding affinity for the same peptide sequence.

In this work, MD simulations augmented with the well-tempered metadynamics (WTM)-[60]nhanced sampling method has been employed to study the adsorption of peptides DDD, DSS, DpSpS, DpSpSGKK, and DpSKGpSK (where pS indicates a phosphorylated serine residue) to both rutile TiO_2 and quartz SiO_2. DDD and DSS represent examples of important binding motifs in the salivary protein statherin and its variants,[61] providing a basis for studying the effects of their phosphorylated counterpart DpSpS which readily binds to the silica surface.[62] The latter two peptides—DpSpSGKK and DpSKGpSK—were designed with the same amino acids arranged in different sequences to determine the effects of peptide sequence on peptide/surface binding, surface-bound conformation, and the extent to which the effects of phosphorylation are influenced by the surrounding amino acid microenvironment. For each system, we determined both the peptide/surface binding free energy and interfacial conformation of the peptide to elucidate key mechanisms of peptide/surface adsorption that could have important implications for future biomaterials and biomedical research.

METHODS

Peptide sequences with N-terminal acetyl (i.e., CH_3CO-) and C-terminal amide (i.e., $-NHCH_3$) capping groups and TiO_2 surface were constructed using the open-source software program Avogadro.[63] Following the protocol used in prior simulations,[50,64] the (100) surface of rutile TiO_2 was simulated with terminal oxygen atoms to mimic a titanium surface in aqueous media at a neutral pH. The surface orientation and degree of cleavage were chosen to be consistent with recent simulations of TiO_2 conducted by Brandt et al.,[49,50] with tri- and doubly coordinated oxygen atoms and with five- and six-coordinated titanium atoms in the top/bottom and bulk layers of the surface, respectively. This mimics TiO_2 in ambient environment, where it tends to be covered with oxygen at physiological pH.[65,66] Furthermore, protonation on the (100) rutile surface at pH = 7 in water is approximately 1% of the O site, which results in less than

DOI: 10.1021/acs.langmuir.8b01392
Langmuir 2019, 35, 5911−5920

Table 1. Details on the Setup of MD Simulations in This Work

simulation	peptide	surface	peptide charge	surface charge	Na^+ ions[a]	box dimensions (nm)
1	DDD	TiO_2	−3	0	3	2.7 × 2.8 × 5.0
2	DSS	TiO_2	−1	0	1	2.7 × 2.8 × 5.0
3	DpSpS	TiO_2	−5	0	5	2.7 × 2.8 × 5.0
4	DDD	SiO_2	−3	−20	23	3.5 × 3.4 × 5.1
5	DSS	SiO_2	−1	−20	21	3.5 × 3.4 × 5.4
6	DpSpS	SiO_2	−5	−20	25	3.5 × 3.4 × 5.4
7	DpSKGpSK	TiO_2	−3	0	3	2.7 × 2.8 × 5.5
8	DpSpSGKK	TiO_2	−3	0	3	2.7 × 2.8 × 5.5
9	DpSKGpSK	SiO_2	−3	−20	23	3.5 × 3.4 × 5.9
10	DpSpSGKK	SiO_2	−3	−20	23	3.5 × 3.4 × 5.9

[a]Includes both surface ions and counterions.

1 OH group on the slab we build. An alternate model for neutral, nonhydroxylated TiO_2 was developed by Předota et al.[47] The short-range interactions between surface oxygens and water oxygens were set equal to the LJ interactions between oxygens in the SPC/E water model; however, the short-ranged interactions between surface titanium atoms and water oxygens were described by a Buckingham potential. In order to describe all short-range interactions by the same potential form, we adopted the LJ parameters fitted from the Buckingham potentials of the MA force field by Brandt and Lyubartsev.[49] The TiO_2 unit cell structure was downloaded from the Crystallography Open Database.[67−70] A TiO_2 supercell 4 × 6 × 9 was built from the unit cell belonging to the space group $P4_2/mnm$, with cell parameters of $a = b = 4.594$ Å and $c = 2.959$ Å. The final cell size used in the MD simulations was ∼2.7 × 2.8 × 1.7 nm with 6 × 9 O site on each face. For SiO_2, a quartz (001) surface was simulated with a Q2 surface environment.[38,56] The surface was prepared from a 7 × 4 × 3 supercell built from an α-quartz (001) rectangular cell provided in the INTERFACE force field,[71] resulting in a final size of ∼3.5 × 3.4 × 2.0 nm used in the simulations. All silicon atoms were hydroxylated with two silanol groups (=$Si(OH)_2$), resulting in 9.4 silanol groups/nm^2. Approximately 1.0 silanol group/nm^2 was ionized to SiO^- with requisite numbers of surface sodium ions added to maintain a neutral interface, mimicking the surface chemistry of quartz in a neutral pH solution.

Visual MD[72] was used to generate simulation boxes with a single peptide placed in a random configuration above each surface in the presence of water. Between 1 and 5 additional sodium ions (termed counterions, in contrast to surface ions) were added to each simulation box to neutralize the charge of the peptide. The z-dimension of each simulation box—between 5.0 and 6.0 nm—was chosen to be large enough to permit accurate binding free energy calculations. Further details of each simulation are included in Table 1. The peptides and counterions were modeled using the CHARMM27 force field,[73] and the TIP3P water model was used to represent water.[74] The force field originally developed by Matsui and Akaogi[39] and fitted into a LJ potential form by Brandt and Lyubartsev[49] is used to model TiO_2, whereas the INTERFACE package developed by Heinz and co-workers—integrated into the CHARMM27 force field—was used to model SiO_2 and surface Na^+ ions.[56] Phosphoserine side chains were fully deprotonated to mimic conditions in a neutral pH environment and were parameterized using a combination of data from Steinbrecher et al.[75] and the CHARMM27 force field.

All simulations were carried out with the GROMACS 5.1.2 MD engine[76] in conjunction with the PLUMED 2.0 plugin.[77] Energy minimization was performed on each system using a steepest descent algorithm for 40 000 steps. The optimized systems were then briefly equilibrated in the *NPT* ensemble for 100 ps at 300 K and 1 bar (semi-isotropic coupling scheme) using the Donadio−Bussi−Parrinello thermostat[78] and Berendsen barostat,[79] respectively. In a subsequent equilibration step, the same thermostat was used to carry out a 100 ps *NVT* simulation at 300 K. A harmonic restraint was placed at 1.8 nm above the surface in simulations 1 through 6 (see Table 1) and 2.2 nm above the surface in simulations 7 through 10. This was done to prevent the peptides from binding to the opposing surface, made possible by the use of periodic boundary conditions in all dimensions. LJ and Coulombic interactions were calculated with a cutoff length of 1.0 nm, and long-range electrostatic interactions were treated with the particle mesh Ewald method. Interactions between hydrogen and other heavy atoms were constrained using the LINCS algorithm[80] to allow for a 2 fs time step to be used in all simulations. To prevent bulk surface distortion, SiO_2 surfaces were frozen apart from the silanol groups in the outer layers that were allowed to fluctuate in position during the simulations. TiO_2 surfaces, lacking OH-termination, were completely frozen in all simulations.

WTM with the multiple walkers method[81] was employed to overcome timescale limitations of classical MD and allow for extensive sampling of the adsorption free energy landscapes of the peptides. Each system consisted of eight replicas with the peptides initially placed in different conformations and at different distances from the surface. A single collective variable (CV) was biased in each simulation, namely, the orthogonal distance between the peptide's center-of-mass (COM) and the surface, with an initial Gaussian hill height of 2.0 kJ/mol and a deposition frequency of 0.5 ps^{-1}. The adjustable WTM parameter (bias factor) was set to 12. The Gaussian hill width, or σ value, ranged from 0.018 to 0.037 nm in each simulation based on the standard deviation of the CV calculated in equilibrium *NVT* simulations of adsorbed peptides. All simulations were carried out to 1 μs/replica (8 μs total sampling) and were deemed converged within this timescale (Figure 1). Convergence was established as the time at which the change in free energy—projected onto the peptide/surface distance—between the adsorbed and solvated states (i.e., the binding energy) ceased to change beyond

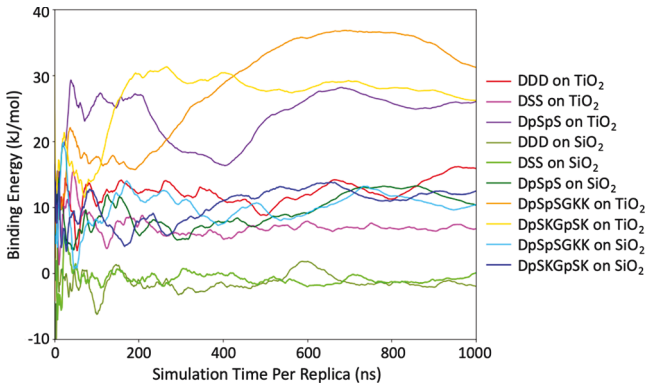

Figure 1. Change in free energy upon peptide/surface adsorption as a function of simulation time per replica for all WTM simulations. The standard deviation of each plot calculated from the last 500 ns of simulations is ±1.78, ±0.32, ±1.18, ±0.75, ±0.32, ±1.66, ±1.56, ±0.76, ±1.37, and ±0.78 kJ/mol. The order of the systems is the same as it appears in Table 1.

DOI: 10.1021/acs.langmuir.8b01392
Langmuir 2019, 35, 5911−5920

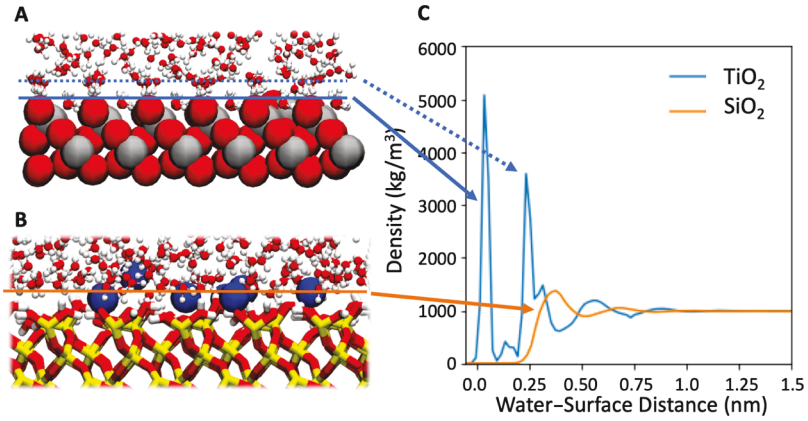

Figure 2. Surface chemistry of TiO_2 and SiO_2: (left) snapshots from WTM simulations of the interfaces between (A) water and TiO_2 and (B) water and SiO_2. (Right) Plot of the water density above the two surfaces as a function of the water−surface orthogonal distance (nm). We note that the bin size of 0.2 A was used to generate (C), and the qualitative conclusions do not change across a wide range of bin sizes. Hydrogen, oxygen, silicon, and titanium atoms are shown in white, red, yellow, and gray coloring, respectively, and sodium ions are shown as blue spheres. For each snapshot, an arrow indicates the value of the water density at the distance indicated by a vertical, dotted line above the surface. For both surfaces, the reference for $z = 0$ is the top frozen atom in the simulation, which is top O and top Si in TiO_2 and SiO_2, respectively.

the level of thermal fluctuations ($kT \approx 2.5$ at 300 K). We use standard equations to calculate the binding free energy, which are discussed in the Supporting Information (Figure S1). Exploration of CV space and evolution of FES is also shown in the Supporting Information (Figure S2).

RESULTS AND DISCUSSION

Surface Chemistry of TiO_2 and SiO_2. In comparing and contrasting peptide adsorption behavior on the two mineral surfaces, it is important to first understand the differences in their surface chemistries to establish a baseline for how these differences might affect our results. TiO_2 and SiO_2 differ in multiple ways. First, TiO_2 is a metal oxide surface in which atoms are generally more ionized than in the SiO_2 surface. This high charge of the titanium atom in TiO_2 results in a well-ordered, zwitterionic-like surface that produces a strong electric field because of the alternating positive and negative charges. Therefore, we might expect much stronger electrostatic interactions between the peptides and TiO_2 versus SiO_2. However, another significant difference between the two surfaces is in their terminal chemistries. At the neutral pH at which the simulations were performed, TiO_2 contains no hydroxyl groups, whereas SiO_2 is fully hydroxylated with some −OH groups partly ionized to O^- (see Methods for more details). Though these conditions largely represent approximations of real conditions (i.e., natural TiO_2 could be partially hydroxylated in some situations, while SiO_2 is not likely to always be fully hydroxylated), our simulations were designed to mimic the true biological conditions and thus could provide important clues into differences in adsorption behavior on the two surfaces.

Figure 2 shows a plot of the water density above each surface as a function of the water−surface distance. Snapshots illustrate the water configurations of the systems near the maximum observed water density above each surface in the WTM simulations. The results show that there are two well-ordered and highly oriented water layers above the TiO_2 surface, indicated by sharp peaks in the density above that of the bulk. The peak positions are in good agreement with a recent MD study.[48] The first layer of water molecules penetrate into the top layer of the surface, driven by electrostatic interactions between water oxygen atoms and surface titanium atoms; formation of the second layer is driven by hydrogen bond interactions between water hydrogen atoms and surface oxygen atoms. Conversely, while the water density is notably higher above the SiO_2 surface than in the bulk solution, the spatial distribution and orientation of water molecules above the surface are relatively random, compared to the TiO_2 surface.

Effects of Phosphorylation on Peptide Adsorption. Binding free energy profiles of the three peptides on the TiO_2 surface are shown in Figure 3A. The results show that DpSpS

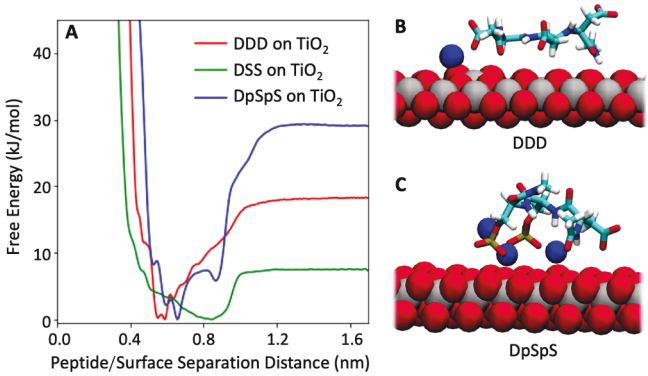

Figure 3. Adsorption of DDD, DSS, and DpSpS on TiO_2: (A) plot of the free energy projected onto the peptide/surface separation distance for the three peptides on TiO_2; (B,C) WTM trajectory snapshots of DDD and DpSpS, respectively, adsorbed to TiO_2, corresponding to the global minimum in (A). Coloring is as described in Figure 2, with the addition of phosphorus atoms shown in gold. Water is not pictured for clarity. Snapshots corresponding to conformations in other local energy minima of all simulated systems are shown in the Supporting Information (Figures S3−S6).

binds most strongly to TiO_2 with a binding free energy of ∼26 kJ/mol. Comparatively, DDD binds nearly 40% weaker to TiO_2 with a binding free energy of ∼16 kJ/mol, and DSS binds with an almost 75% decrease in binding free energy compared to DpSpS at ∼7 kJ/mol. Notably, the percent differences in the binding free energies of the three peptides are nearly the same as the differences in their net charges: DpSpS, with a net charge of +5, has a 40% higher overall charge than DDD (+3)

DOI: 10.1021/acs.langmuir.8b01392
Langmuir 2019, 35, 5911−5920

and an 80% higher charge than DSS (+1), demonstrating a strong electrostatic driving force for peptide adsorption to TiO_2.

Visual analysis of the trajectories provides a molecular basis for the observed trend in peptide binding strength to TiO_2. Figure 3B,C shows snapshots of peptides DDD and DpSpS, respectively, adsorbed to the TiO_2 surface. While all three aspartate and/or pS residues in the peptide sequences are bound to the surface in each case, DDD appears to adopt a more flattened conformation on the surface, consistent with the results of Figure 3B, which show that the COM of DDD is able to bind slightly closer to the surface than that of DpSpS. However, stronger electrostatic interactions between pS residues (−2.0 charge) in DpSpS and Ti atoms (+2.2 charge) in TiO_2 dominate the nature of binding to TiO_2 and lead to a higher overall binding free energy than for DDD on TiO_2. This is despite the presence of surface oxygen atoms (−1.1 charge) that serve to weakly screen the highly charged Ti atoms from the pS residues, which seek to fully compensate their charge by coordinating with nearby sodium atoms from solution, as shown in Figure 3C. In the case of DSS, the only electrostatic interaction with the surface comes from the lone aspartate, resulting in a much lower binding free energy to TiO_2 than for the other two peptides.

The binding free energy profiles of the peptides on SiO_2 (Figure 4A) show the same enhanced surface binding strength

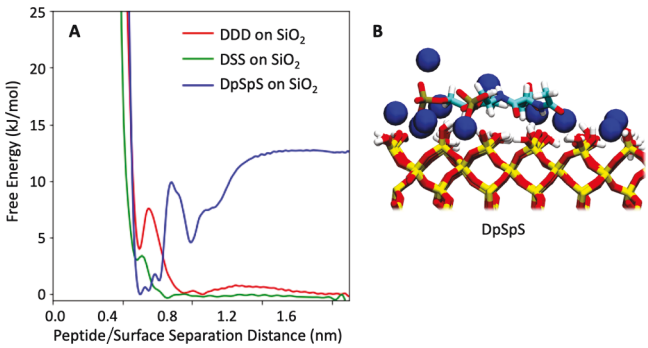

Figure 4. Adsorption of DDD, DSS, and DpSpS on SiO_2: (A) plot of the free energy projected onto the peptide/surface separation distance for the three peptides on SiO_2; (B) WTM trajectory snapshot of DpSpS adsorbed to SiO_2. Coloring is as described in Figure 2, with the addition of phosphorus atoms shown in gold. Water is not pictured for clarity.

with sequence phosphorylation as on the TiO_2 surface, though for different reasons, as discussed below. In the case of all three peptides, there is an energy barrier to adsorb onto the surface. However, for DDD and DSS, the results show that even if the peptides are able to cross this barrier to adsorption, it is energetically preferable for the peptides to remain in the bulk solution. Conversely, DpSpS has a binding free energy of ∼12 kJ/mol to SiO_2, though, notably, this is only about half the value on TiO_2. This reduction in binding free energy is due to a different, less effective binding mechanism of DpSpS on SiO_2 compared to that on TiO_2. In SiO_2, the hydroxyl groups (both OH− and O−) that are allowed to fluctuate in position during the simulation effectually shield the charge of the Si atoms below them (+1.1 charge), preventing the negatively charged aspartate and pS residues in the peptides from binding to the Si atoms. Sodium ions with a +1.0 charge adsorb onto surface sites of ionized oxygen atoms (−0.9 charge), which, unable to compensate for the full charge of the sodium ions, provide weak binding sites for positively charged peptide residues to adsorb. This ion-mediated binding mechanism is the primary means by which pS residues are able to bind to the SiO_2 surface, as shown in Figure 4B. As with adsorption to TiO_2, pS residues also coordinate with sodium ions from the solution to further compensate for their −2.0 charge. In the case of DDD and DSS, visual analysis of the trajectories confirms that the peptides are unable to bind to the surface via this same ion-mediated binding mechanism. The natural salivary statherin fragment SN15 and its motifs where the DpSpS sequence of SN15 is mutated to DSS(SN_S15) and DDD(SN_A15) has shown a similar trend of decrease in binding energy with decreasing charge, when interacting with the hydroxyapatite surface.[61] Charged residues are also found to be essential in the binding of the Ti-binding peptide RKLPDA to the TiO_2(110) surface.[82,83] For example, in a study by Walsh et al.,[18] the detachment of the RKLPDA peptide is observed after mutation of charged residue Asp to Ala.

We also note that influence of charge comes from not only the peptide but also the mediating ions on the surface. Desmond et al.[84] simulated positively charged alkylammonium adhesion to silica in four different electrolytes and found that Ca^{2+} coordinated to the negatively charged O site has greater adsorption compared to monovalent electrolytes, proving that ions can strongly influence peptide binding to a surface.

Figure 5 shows the comparison of the binding energy across the tripeptide−surface systems. In general, it is seen that the

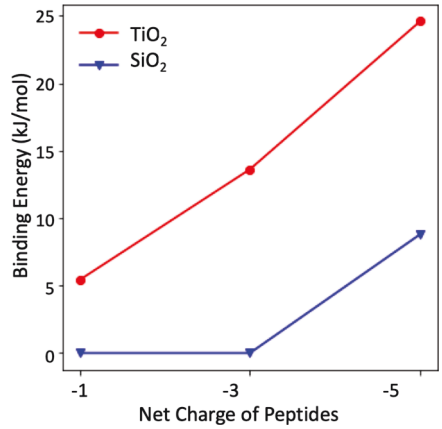

Figure 5. Binding energy as a function of peptide charge for DDD, DSS, and DpSpS on TiO_2 and SiO_2 as labeled. Charges are −1, −3, and −5 for DDD, DSS, and DpSpS, respectively.

binding energy of peptides increases with peptide charge. This trend is more pronounced for TiO_2 than for SiO_2. For the binding of peptides to SiO_2, it is seen that there is a minimum charge threshold below which the peptides do not bind to the silica surface, and DpSpS has the highest binding energy, which indicates that the strong binding driving force is induced by phosphorylation.

However, this phenomenon of phosphorylation increasing binding is in apparent contradiction to a recent MD study by Sprenger et al.,[16] in which it was found that phosphorylation plays an opposite role in R5, a 19-residue native silaffin-based peptide, binding to silica. In the case of R5, three instances of phosphorylation were considered ranging from none to complete phosphorylation of seven residues. In this case, it was determined that phosphorylation decreases the binding of

DOI: 10.1021/acs.langmuir.8b01392
Langmuir 2019, 35, 5911−5920

the peptide to silica in contrast to our observations reported above. The difference is due to some of the intrinsic differences between 19-residue R5 and the nature-inspired mini-peptides based on SN15. In particular, the increase in phosphorylation in the case of R5 leads to substantive disruption of the C-terminal motif (RRIL domain), which has been strongly implicated as a binding region in R5.[85] Additionally, the simple sequence of the peptides considered here allows for a strong Na^+-mediated binding mechanism. Although the peptides are negatively charged and bind to negatively charged silica, the cation mediation of the binding mechanism is sufficient to account for the apparent increase in peptide binding free energy. This further underscores our findings about the impact of peptide sequence on peptide binding energy.

Effects of Peptide Sequence on Surface Adsorption. To explore the effects of peptide sequence on surface adsorption and in particular, the effects on the ability of pS residues to increase the strength of mineral oxide binding, we designed two additional peptides with the same residue composition and a net charge of −3 (n.b., same as that for DDD) but with slightly different sequences. The new peptides were capped on the N and C termini in the manner of all previously studied peptides. In the first peptide sequence, DpSpSGKK, two pS residues are placed next to each other as they were in the previously studied peptide, DpSpS. In the second peptide sequence, DpSKGpSK, the latter pS residue is exchanged with a lysine (K) residue further down in the sequence so that both pS residues neighbor a positively charged lysine residue.

Figure 6A shows the binding free energy profiles of the two peptides on the TiO_2 surface, with corresponding snapshots of adsorbed peptide conformations (Figure 6B,C). The results show that consistent with our earlier findings, a small negatively charged peptide with pS residues binds strongly to a TiO_2 surface at physiological conditions. DpSpSGKK binds with a free energy of ∼35 kJ/mol, which is 9 kJ/mol higher than the binding free energy found for DpSpS on TiO_2, likely due to the addition of beneficial lysine/surface−O interactions. Figure 6A shows that the binding free energy of DpSKGpSK on TiO_2 is less than for DpSpSGKK on TiO_2 by ∼5 kJ/mol or by ∼14%. This implies that differences in local electrostatic driving forces centered around the pS residues (i.e., different sequences) lead to differential peptide/surface binding because the overall charge of the peptides remains the same at −3. Rearranging the peptide sequence to have lysine residues directly next to pS residues results in a slight charge-dampening effect that marginally reduces local electrostatic driving forces and leads to a lower binding free energy. Importantly, the percent decrease in binding free energy in going from DpSpSGKK to DpSKGpSK on TiO_2 (∼14%) is much smaller than the decrease in going from DpSpS to DDD on TiO_2 (∼40%), discussed earlier, even though the local charge distributions are very similar for the peptides [i.e., the local collective charge of pS and K residues in DpSKGpSK (−2 + 1 = −1) is the same as for D in DDD (−1)]. This indicates that the global or overall electrostatic driving force also plays an important role in peptide/TiO_2 binding, because in going from DpSpSGKK to DpSKGpSK, the net charge remains the same at −3, whereas in going from DpSpS to DDD, the net charge decreases from −5 to −3.

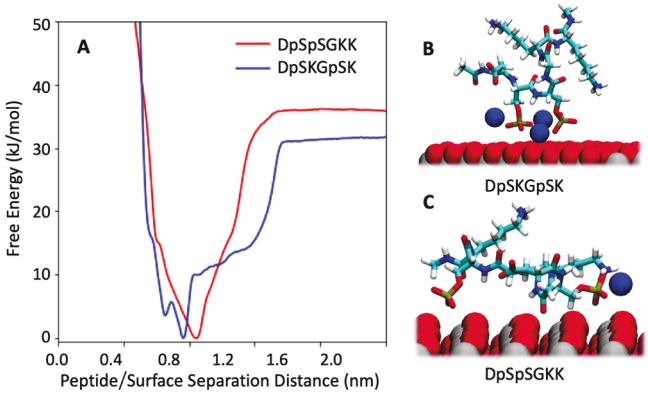

Figure 6. Adsorption of DpSpSGKK and DpSKGpSK on TiO_2: (A) plot of the free energy projected onto the peptide/surface separation distance for the two peptides on TiO_2; (B,C) WTM trajectory snapshots of DpSpSGKK and DpSKGpSK, respectively, adsorbed to TiO_2. Coloring is as described in Figure 2, with the addition of phosphorus atoms shown in gold. Water is not pictured for clarity.

A conformational analysis of DpSpSGKK and DpSKGpSK bound to TiO_2 (Figure 6B,C) shows many similarities to earlier results for DpSpS and DDD on TiO_2 (Figure 3B,C). For instance, when pS residues are next to each other in the sequence, the peptide adopts a more compact structure that leads to an energy minimum further out from the surface, and when pS residues are separated from one another (or gone altogether in the case of DDD), the peptide adopts a more flattened conformation that allows it to approach closer to the surface. Differences arise amid the profiles of DpSKGpSK and DpSpSGKK between a peptide/surface distance of ∼0.8 and 1.3 nm (Figure 6A), where a small shoulder appears for DpSKGpSK that is not seen for DpSpSGKK. Investigation of the simulation trajectory for DpSKGpSK on TiO_2 in this distance window indicates that the shoulder behavior is largely due to configurations where only one of the two pS residues is bound to the surface. The reduction in electrostatic interactions of these surface-bound configurations is reflected in a reduced binding free energy between 10 and 20 kJ/mol (Figure 6A) or approximately half of the binding free energy when both pS residues bind to the surface. No equivalent shoulder behavior is observed for DpSpSGKK on TiO_2 because the close proximity of the two pS residues serves to stabilize each other on the surface.

Figure 7A shows the binding free energy profiles of DpSpSGKK and DpSKGpSK on the SiO_2 surface, with corresponding snapshots of adsorbed peptide conformations (Figure 7B,C). The results show that even with the net charged reduced from −5 to −3 with the incorporation of the two lysine residues, both peptides bind strongly to the SiO_2 surface, which is a departure from the behavior of DDD, also with a charge of −3, for which it was energetically preferable to remain in bulk solution rather than adsorb onto the SiO_2 surface. As shown in Figure 7B,C, this is because the peptides are still able to bind to SiO_2 via the ion-mediated binding mechanism discussed earlier, despite the charge-dampening effects of the neighboring lysine residues. Figure 7A shows that DpSpSGKK binds with an adsorption free energy of ∼14 kJ/mol, which is slightly higher than the binding free energy of ∼12 kJ/mol that was found earlier for DpSpS on SiO_2 (Figure 4A). Additional electrostatic interactions may be possible with the addition of the lysine residues in DpSpSGKK, but in general, the results show that the interactions between pS residues and surface-bound ions dominate the adsorption

DOI: 10.1021/acs.langmuir.8b01392
Langmuir 2019, 35, 5911−5920

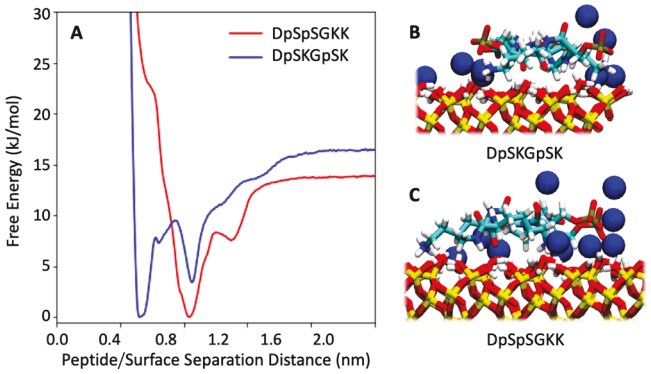

Figure 7. Adsorption of DpSpSGKK and DpSKGpSK on SiO_2: (A) plot of the free energy projected onto the peptide/surface separation distance for the two peptides on SiO_2; (B,C) WTM trajectory snapshots of DpSpSGKK and DpSKGpSK, respectively, from the first minimum in each energy profile adsorbed to SiO_2. Coloring is as described in Figure 2, with the addition of phosphorus atoms shown in gold. Water is not pictured for clarity.

behavior of the peptides and lead to their similar binding free energies on SiO_2. In contrast with the behavior on the TiO_2 surface (Figure 6A), the binding free energy of DpSKGpSK at ~16 kJ/mol is slightly higher than that of DpSpSGKK on SiO_2, further demonstrating that the ability of the pS residues to bind to surface-bound sodium ions on SiO_2 is not negatively impacted by the presence of neighboring lysine residues. Consistent with previous findings (Figures 3 and 6), separating out the pS residues in the peptide sequence allows the peptide to adopt a more flattened conformation at a distance closer to the surface (Figures 7A,C). Combined with the fact that ion-mediated binding is not hindered by adjacent positive charges in the sequence, this explains the minor increase in the binding free energy of DpSKGpSK on SiO_2 compared to that in DpSpSGKK and the opposite trend in the free energy of binding to the TiO_2 surface. To address the impact of sequence in biorecognition, Mitternacht et al.[86] have performed atomic-level simulation of a 12-residue peptide S1 (AQNPSDNNTHTH) and its random permutation sequence S3 (same amino acid composition as S1 but in a different order) and found that S1 has more peptide adhesion to gallium arsenide and silica surfaces. They suggested that change of proline position in the sequence results in the change of binding. In the current work as well, we find that it is the relative position between charged residues that impacts peptide/surface adhesion.

CONCLUSIONS

This study investigated the primary molecular driving forces underlying peptide adsorption to metal oxide surfaces, specifically the effects of (1) surface chemistry, (2) serine phosphorylation, and (3) peptide sequence, on the binding free energy of the peptides and their equilibrium adsorbed-state conformations. Inspired by the binding motif in mineral precipitating proteins, we varied both the number and position of pS residues in five synthetically designed peptide sequences. Varying the number of pS residues (i.e., the overall negative charge of the peptides) led to the finding that electrostatic interactions are a strong driving force for adsorption to both TiO_2 and SiO_2. Despite distinct surface chemistries, an increased degree of serine phosphorylation was found to significantly enhance peptide adsorption on both surfaces. However, our results point to different mechanisms of electrostatically driven peptide binding to the two surfaces: although negatively charged peptide residues such as pS bind to highly charged Ti atoms on the TiO_2 surface, they bind to the hydroxylated SiO_2 surface via an ion-mediated binding mechanism (i.e., Na^+ ions adsorbed onto ionized OH groups). The latter mechanism of binding to the SiO_2 surface resulted in weaker peptide/surface binding strengths than adsorption onto the TiO_2 surface. In addition, our results showed that it is not only the global electrostatic environment that determines the strength and manner of peptide binding to metal oxide surfaces but also local electrostatic interactions between the peptide and surface. Simulations were performed of two peptides with the same overall negative charge and residue composition but with pS residues arranged in different locations throughout the peptides' sequences. While the peptides were observed to bind via the same mechanisms as described above to each of the surfaces, differently arranged sequences resulted in unique peptide/surface binding energies and peptide adsorption conformations on the two surfaces. By studying such synthetically designed peptide sequences, we largely simplified the peptide/surface binding scenario. This allowed us to isolate the impacts of surface chemistry, phosphorylation, and peptide sequence on binding, providing new and important insights into the process of peptide adsorption onto metal oxide surfaces. In future work, we will extend the above findings to more complex protein/surface systems, in order to further enhance our understanding of protein−mineral interactions for use in a wide variety of applications and new biobased technologies.

ASSOCIATED CONTENT

Supporting Information

The Supporting Information is available free of charge on the ACS Publications website at DOI: 10.1021/acs.langmuir.8b01392.

Plot of the energy projected onto the peptide/surface separation distance for all the simulated systems at the end of simulation; boundary of adsorption and solvation region in 10 simulation systems; analysis of simulation convergence of DDD, DpSpS, and DpSpSGKK; free energy profile and snapshots of the peptide/surface interface; and binding energy for DDD, DpSKGpSK, and DpSpSGKK on TiO_2 and SiO_2 as labeled (PDF)

AUTHOR INFORMATION

Corresponding Author

*E-mail: jpfaendt@uw.edu. Phone: (206) 616-8128.

ORCID

Gary Drobny: 0000-0002-7293-1897

Jim Pfaendtner: 0000-0001-6727-2957

Notes

The authors declare no competing financial interest.

ACKNOWLEDGMENTS

The authors acknowledge support of NSF award MCB-1715123 and NIH award 1R21DE026959-01. This work was facilitated using computational, storage, and networking infrastructure provided by the Hyak supercomputer system, supported in part by the University of Washington and the

DOI: 10.1021/acs.langmuir.8b01392
Langmuir 2019, 35, 5911−5920

UW Student Technology Fee Proposal program (award 2015-028) and NSF MRI program CHE-1624430.

REFERENCES

(1) Fernandez-Fernandez, A.; Manchanda, R.; McGoron, A. J. Theranostic Applications of Nanomaterials in Cancer: Drug Delivery, Image-Guided Therapy, and Multifunctional Platforms. *Appl. Biochem. Biotechnol.* **2011**, *165*, 1628−1651.

(2) Mahmood, M.; Casciano, D.; Xu, Y.; Biris, A. S. Engineered Nanostructural Materials for Application in Cancer Biology and Medicine. *J. Appl. Toxicol.* **2012**, *32*, 10−19.

(3) Care, A.; Bergquist, P. L.; Sunna, A. Solid-Binding Peptides: Smart Tools for Nanobiotechnology. *Trends Biotechnol.* **2015**, *33*, 259−268.

(4) Liu, Q.; Wang, J.; Boyd, B. J. Peptide-Based Biosensors. *Talanta* **2015**, *136*, 114−127.

(5) Park, S.; Lee, H.; Lee, S.-Y. Effect of Peptide Conformation on TiO_2 biomineralization. *Dalton Trans.* **2013**, *42*, 13817−13820.

(6) Puddu, V.; Slocik, J. M.; Naik, R. R.; Perry, C. C. Titania Binding Peptides as Templates in the Biomimetic Synthesis of Stable Titania Nanosols: Insight into the Role of Buffers in Peptide-Mediated Mineralization. *Langmuir* **2013**, *29*, 9464−9472.

(7) Sarikaya, M.; Tamerler, C.; Jen, A. K.-Y.; Schulten, K.; Baneyx, F. Molecular Biomimetics: Nanotechnology through Biology. *Nat. Mater.* **2003**, *2*, 577−585.

(8) Merrill, N. A.; Nitka, T. T.; McKee, E. M.; Merino, K. C.; Drummy, L. F.; Lee, S.; Reinhart, B.; Ren, Y.; Munro, C. J.; Pylypenko, S.; et al. Effects of Metal Composition and Ratio on Peptide-Templated Multimetallic PdPt Nanomaterials. *ACS Appl. Mater. Interfaces* **2017**, *9*, 8030−8040.

(9) Luan, B.; Huynh, T.; Zhao, L.; Zhou, R. Potential Toxicity of Graphene to Cell Functions via Disrupting Protein-Protein Interactions. *ACS Nano* **2015**, *9*, 663−669.

(10) Nel, A.; Xia, T.; Mädler, L.; Li, N. Toxic Potential of Materials at the Nanolevel. *Science* **2006**, *311*, 622−627.

(11) Walsh, T. R. Pathways to Structure-Property Relationships of Peptide-Materials Interfaces: Challenges in Predicting Molecular Structures. *Acc. Chem. Res.* **2017**, *50*, 1617−1624.

(12) Walsh, T. R.; Knecht, M. R. Biointerface Structural Effects on the Properties and Applications of Bioinspired Peptide-Based Nanomaterials. *Chem. Rev.* **2017**, *117*, 12641−12704.

(13) Latour, R. A., Jr. Biomaterials: Protein−Surface Interactions. *Encyclopedia of Biomaterials and Biomedical Engineering*; CRC Press, 2005; pp 270−278.

(14) Gray, J. J. The Interaction of Proteins with Solid Surfaces. *Curr. Opin. Struct. Biol.* **2004**, *14*, 110−115.

(15) Marichal, L.; Renault, J.-P.; Chédin, S.; Lagniel, G.; Klein, G.; Aude, J.-C.; Tellier-Lebegue, C.; Armengaud, J.; Pin, S.; Labarre, J.; et al. Importance of Post-Translational Modifications in the Interaction of Proteins with Mineral Surfaces: The Case of Arginine Methylation and Silica Surfaces. *Langmuir* **2018**, *34*, 5312−5322.

(16) Sprenger, K. G.; Prakash, A.; Drobny, G.; Pfaendtner, J. Investigating the Role of Phosphorylation in the Binding of Silaffin Peptide R5 to Silica with Molecular Dynamics Simulations. *Langmuir* **2018**, *34*, 1199−1207.

(17) Zhao, W.; Xu, Z.; Cui, Q.; Sahai, N. Predicting the Structure-Activity Relationship of Hydroxyapatite-Binding Peptides by Enhanced-Sampling Molecular Simulation. *Langmuir* **2016**, *32*, 7009−7022.

(18) Skelton, A. A.; Liang, T.; Walsh, T. R. Interplay of Sequence, Conformation, and Binding at the Peptide−Titania Interface as Mediated by Water. *ACS Appl. Mater. Interfaces* **2009**, *1*, 1482−1491.

(19) Sultan, A. M.; Westcott, Z. C.; Hughes, Z. E.; Palafox-Hernandez, J. P.; Giesa, T.; Puddu, V.; Buehler, M. J.; Perry, C. C.; Walsh, T. R. Aqueous Peptide-TiO_2 Interfaces: Isoenergetic Binding via Either Entropically or Enthalpically Driven Mechanisms. *ACS Appl. Mater. Interfaces* **2016**, *8*, 18620−18630.

(20) Hughes, Z. E.; Kochandra, R.; Walsh, T. R. Facet-Specific Adsorption of Tripeptides at Aqueous Au Interfaces: Open Questions in Reconciling Experiment and Simulation. *Langmuir* **2017**, *33*, 3742−3754.

(21) Carravetta, V.; Monti, S. Peptide-TiO_2 Surface Interaction in Solution by AB Initio and Molecular Dynamics Simulations. *J. Phys. Chem. B* **2006**, *110*, 6160−6169.

(22) Vellore, N. A.; Yancey, J. A.; Collier, G.; Latour, R. A.; Stuart, S. J. Assessment of the Transferability of a Protein Force Field for the Simulation of Peptide-Surface Interactions. *Langmuir* **2010**, *26*, 7396−7404.

(23) Wei, S.; Knotts, T. A., IV A Coarse Grain Model for Protein-Surface Interactions. *J. Chem. Phys.* **2013**, *139*, 095102.

(24) Wei, Y.; Latour, R. A. Benchmark Experimental Data Set and Assessment of Adsorption Free Energy for Peptide-Surface Interactions. *Langmuir* **2009**, *25*, 5637−5646.

(25) Tan, Y. N.; Lee, J. Y.; Wang, D. I. C. Uncovering the Design Rules for Peptide Synthesis of Metal Nanoparticles. *J. Am. Chem. Soc.* **2010**, *132*, 5677−5686.

(26) Hnilova, M.; Oren, E. E.; Seker, U. O. S.; Wilson, B. R.; Collino, S.; Evans, J. S.; Tamerler, C.; Sarikaya, M. Effect of Molecular Conformations on the Adsorption Behavior of Gold-Binding Peptides. *Langmuir* **2008**, *24*, 12440−12445.

(27) Ozboyaci, M.; Kokh, D. B.; Corni, S.; Wade, R. C. Modeling and Simulation of Protein-Surface Interactions: Achievements and Challenges. *Q. Rev. Biophys.* **2016**, *49*, No. e4.

(28) Liu, S.; Meng, X.-Y.; Perez-Aguilar, J. M.; Zhou, R. An in Silico Study of TiO_2 nanoparticles Interaction with Twenty Standard Amino Acids in Aqueous Solution. *Sci. Rep.* **2016**, *6*, 37761.

(29) Friedrichs, W.; Köppen, S.; Langel, W. Titanium Binding Dodecapeptides and the Impact of Water Structure. *Surf. Sci.* **2013**, *617*, 42−52.

(30) Friedrichs, W.; Langel, W. Atomistic Modeling of Peptide Adsorption on Rutile (100) in the Presence of Water and of Contamination by Low Molecular Weight Alcohols. *Biointerphases* **2014**, *9*, 031006.

(31) Emami, F. S.; Puddu, V.; Berry, R. J.; Varshney, V.; Patwardhan, S. V.; Perry, C. C.; Heinz, H. Prediction of Specific Biomolecule Adsorption on Silica Surfaces as a Function of PH and Particle Size. *Chem. Mater.* **2014**, *26*, 5725−5734.

(32) Sultan, A. M.; Hughes, Z. E.; Walsh, T. R. Binding Affinities of Amino Acid Analogues at the Charged Aqueous Titania Interface: Implications for Titania-Binding Peptides. *Langmuir* **2014**, *30*, 13321−13329.

(33) Hayashi, T.; Sano, K.-I.; Shiba, K.; Iwahori, K.; Yamashita, I.; Hara, M. Critical Amino Acid Residues for the Specific Binding of the Ti-Recognizing Recombinant Ferritin with Oxide Surfaces of Titanium and Silicon. *Langmuir* **2009**, *25*, 10901−10906.

(34) Dickerson, M. B.; Jones, S. E.; Cai, Y.; Ahmad, G.; Naik, R. R.; Kröger, N.; Sandhage, K. H. Identification and Design of Peptides for the Rapid, High-Yield Formation of Nanoparticulate TiO_2 from Aqueous Solutions at Room Temperature. *Chem. Mater.* **2008**, *20*, 1578−1584.

(35) Thingholm, T. E.; Jørgensen, T. J. D.; Jensen, O. N.; Larsen, M. R. Highly Selective Enrichment of Phosphorylated Peptides Using Titanium Dioxide. *Nat. Protoc.* **2006**, *1*, 1929−1935.

(36) Vertegel, A. A.; Siegel, R. W.; Dordick, J. S. Silica Nanoparticle Size Influences the Structure and Enzymatic Activity of Adsorbed Lysozyme. *Langmuir* **2004**, *20*, 6800−6807.

(37) Puddu, V.; Perry, C. C. Peptide Adsorption on Silica Nanoparticles: Evidence of Hydrophobic Interactions. *ACS Nano* **2012**, *6*, 6356−6363.

(38) Patwardhan, S. V.; Emami, F. S.; Berry, R. J.; Jones, S. E.; Naik, R. R.; Deschaume, O.; Heinz, H.; Perry, C. C. Chemistry of Aqueous Silica Nanoparticle Surfaces and the Mechanism of Selective Peptide Adsorption. *J. Am. Chem. Soc.* **2012**, *134*, 6244−6256.

(39) Matsui, M.; Akaogi, M. Molecular Dynamics Simulation of the Structural and Physical Properties of the Four Polymorphs of TiO_2. *Mol. Simul.* **1991**, *6*, 239−244.

(40) Ferrante, T. Free-Living Amoebae: Pathogenicity and Immunity. *Parasite Immunol.* **1991**, *13*, 31−47.

DOI: 10.1021/acs.langmuir.8b01392
Langmuir 2019, 35, 5911−5920

(41) Emami, F. S.; Puddu, V.; Berry, R. J.; Varshney, V.; Patwardhan, S. V.; Perry, C. C.; Heinz, H. Prediction of Specific Biomolecule Adsorption on Silica Surfaces as a Function of PH and Particle Size. *Chem. Mater.* **2014**, *26*, 5725−5734.
(42) Kroutil, O.; Chval, Z.; Skelton, A. A.; Předota, M. Computer Simulations of Quartz (101)-Water Interface over a Range of PH Values. *J. Phys. Chem. C* **2015**, *119*, 9274−9286.
(43) Ozboyaci, M.; Kokh, D. B.; Corni, S.; Wade, R. C. Modeling and Simulation of Protein-Surface Interactions: Achievements and Challenges. *Q. Rev. Biophys.* **2016**, *49*, No. e4.
(44) Harding, J. H.; Duffy, D. M.; Sushko, M. L.; Rodger, P. M.; Quigley, D.; Elliott, J. A. Computational Techniques at the Organic−Inorganic Interface in Biomineralization. *Chem. Rev.* **2008**, *108*, 4823−4854.
(45) De Angelis, F.; Di Valentin, C.; Fantacci, S.; Vittadini, A.; Selloni, A. Theoretical Studies on Anatase and Less Common TiO_2 phases: Bulk, Surfaces, and Nanomaterials. *Chem. Rev.* **2014**, *114*, 9708−9753.
(46) Zhang, H.; Banfield, J. F. Structural Characteristics and Mechanical and Thermodynamic Properties of Nanocrystalline TiO_2. *Chem. Rev.* **2014**, *114*, 9613−9644.
(47) Předota, M.; Bandura, A. V.; Cummings, P. T.; Kubicki, J. D.; Wesolowski, D. J.; Chialvo, A. A.; Machesky, M. L. Electric Double Layer at the Rutile (110) Surface. 1. Structure of Surfaces and Interfacial Water from Molecular Dynamics by Use of Ab Initio Potentials. *J. Phys. Chem. B* **2004**, *108*, 12049−12060.
(48) Friedrichs, W.; Langel, W. Atomistic Modeling of Peptide Adsorption on Rutile (100) in the Presence of Water and of Contamination by Low Molecular Weight Alcohols. *Biointerphases* **2014**, *9*, 031006.
(49) Brandt, E. G.; Lyubartsev, A. P. Systematic Optimization of a Force Field for Classical Simulations of TiO_2-Water Interfaces. *J. Phys. Chem. C* **2015**, *119*, 18110−18125.
(50) Brandt, E. G.; Lyubartsev, A. P. Molecular Dynamics Simulations of Adsorption of Amino Acid Side Chain Analogues and a Titanium Binding Peptide on the TiO2 (100) Surface. *J. Phys. Chem. C* **2015**, *119*, 18126−18139.
(51) Köppen, S.; Langel, W. Simulation of the interface of (100) rutile with aqueous ionic solution. *Surf. Sci.* **2006**, *600*, 2040−2050.
(52) Jones, J. E. On the Determination of Molecular Fields. II. From the Equation of State of a Gas. *Proc. R. Soc. A* **1924**, *106*, 463−477.
(53) Steinbrecher, T.; Latzer, J.; Case, D. A. Revised AMBER Parameters for Bioorganic Phosphates. *J. Chem. Theory Comput.* **2012**, *8*, 4405−4412.
(54) Brooks, B. R.; Brooks, C. L.; Mackerell, A. D.; Nilsson, L.; Petrella, R. J.; Roux, B.; Won, Y.; Archontis, G.; Bartels, C.; Boresch, S.; et al. CHARMM: The Biomolecular Simulation Program. *J. Comput. Chem.* **2009**, *30*, 1545−1614.
(55) Rimola, A.; Costa, D.; Sodupe, M.; Lambert, J.-F.; Ugliengo, P. Silica Surface Features and Their Role in the Adsorption of Biomolecules: Computational Modeling and Experiments. *Chem. Rev.* **2013**, *113*, 4216−4313.
(56) Emami, F. S.; Puddu, V.; Berry, R. J.; Varshney, V.; Patwardhan, S. V.; Perry, C. C.; Heinz, H. Force Field and a Surface Model Database for Silica to Simulate Interfacial Properties in Atomic Resolution. *Chem. Mater.* **2014**, *26*, 2647−2658.
(57) Walsh, T. R. Pathways to Structure-Property Relationships of Peptide-Materials Interfaces: Challenges in Predicting Molecular Structures. *Acc. Chem. Res.* **2017**, *50*, 1617−1624.
(58) Latour, R. A. Molecular Simulation of Protein-Surface Interactions: Benefits, Problems, Solutions, and Future Directions (Review). *Biointerphases* **2008**, *3*, FC2−FC12.
(59) Lutz, H.; Jaeger, V.; Schmüser, L.; Bonn, M.; Pfaendtner, J.; Weidner, T. The Structure of the Diatom Silaffin Peptide R5 within Freestanding Two-Dimensional Biosilica Sheets. *Angew. Chem., Int. Ed.* **2017**, *56*, 8277−8280.
(60) Barducci, A.; Bussi, G.; Parrinello, M. Well-Tempered Metadynamics: A Smoothly Converging and Tunable Free-Energy Method. *Phys. Rev. Lett.* **2008**, *100*, 020603.
(61) Raj, P. A.; Johnsson, M.; Levine, M. J.; Nancollas, G. H. Salivary statherin. Dependence on sequence, charge, hydrogen bonding potency, and helical conformation for adsorption to hydroxyapatite and inhibition of mineralization. *J. Biol. Chem.* **1992**, *267*, 5968−5976.
(62) Santos, O.; Kosoric, J.; Hector, M. P.; Anderson, P.; Lindh, L. Adsorption Behavior of Statherin and a Statherin Peptide onto Hydroxyapatite and Silica Surfaces by in Situ Ellipsometry. *J. Colloid Interface Sci.* **2008**, *318*, 175−182.
(63) Hanwell, M. D.; Curtis, D. E.; Lonie, D. C.; Vandermeerschd, T.; Zurek, E.; Hutchison, G. R. Avogadro: An Advanced Semantic Chemical Editor, Visualization, and Analysis Platform. *J. Cheminf.* **2012**, *4*, 17.
(64) Healy, K. E.; Ducheyne, P. Hydration and Preferential Molecular Adsorption on Titanium in Vitro. *Biomaterials* **1992**, *13*, 553−561.
(65) Roddick-Lanzilotta, A. D.; Connor, P. A.; McQuillan, A. J. An In Situ Infrared Spectroscopic Study of the Adsorption of Lysine to TiO2 from an Aqueous Solution. *Langmuir* **1998**, *14*, 6479−6484.
(66) Healy, K. E.; Ducheyne, P. Hydration and Preferential Molecular Adsorption on Titanium in Vitro. *Biomaterials* **1992**, *13*, 553−561.
(67) Merkys, A.; Vaitkus, A.; Butkus, J.; Okulič-Kazarinas, M.; Kairys, V.; Gražulis, S. COD::CIF::Parser: An Error-Correcting CIF Parser for the Perl Language. *J. Appl. Crystallogr.* **2016**, *49*, 292−301.
(68) Gražulis, S.; Merkys, A.; Vaitkus, A.; Okulič-Kazarinas, M. Computing Stoichiometric Molecular Composition from Crystal Structures. *J. Appl. Crystallogr.* **2015**, *48*, 85−91.
(69) Gražulis, S.; Chateigner, D.; Downs, R. T.; Yokochi, A. F. T.; Quirós, M.; Lutterotti, L.; Manakova, E.; Butkus, J.; Moeck, P.; Le Bail, A. Crystallography Open Database - An Open-Access Collection of Crystal Structures. *J. Appl. Crystallogr.* **2009**, *42*, 726−729.
(70) Gražulis, S.; Daškevič, A.; Merkys, A.; Chateigner, D.; Lutterotti, L.; Quirós, M.; Serebryanaya, N. R.; Moeck, P.; Downs, R. T.; Le Bail, A. Crystallography Open Database (COD): An Open-Access Collection of Crystal Structures and Platform for World-Wide Collaboration. *Nucleic Acids Res.* **2012**, *40*, D420−D427.
(71) Lin, T.-J.; Heinz, H. Accurate Force Field Parameters and PH Resolved Surface Models for Hydroxyapatite to Understand Structure, Mechanics, Hydration, and Biological Interfaces. *J. Phys. Chem. C* **2016**, *120*, 4975−4992.
(72) Humphrey, W.; Dalke, A.; Schulten, K. VMD: Visual Molecular Dynamics. *J. Mol. Graphics* **1996**, *14*, 33−38.
(73) Foloppe, N.; MacKerell, A. D., Jr. All-Atom Empirical Force Field for Nucleic Acids: I. Parameter Optimization Based on Small Molecule and Condensed Phase Macromolecular Target Data. *J. Comput. Chem.* **2000**, *21*, 86−104.
(74) Jorgensen, W. L.; Chandrasekhar, J.; Madura, J. D.; Impey, R. W.; Klein, M. L. Comparison of Simple Potential Functions for Simulating Liquid Water. *J. Chem. Phys.* **1983**, *79*, 926−935.
(75) Steinbrecher, T.; Latzer, J.; Case, D. A. Revised AMBER Parameters for Bioorganic Phosphates. *J. Chem. Theory Comput.* **2012**, *8*, 4405−4412.
(76) Abraham, M. J.; Murtola, T.; Schulz, R.; Páll, S.; Smith, J. C.; Hess, B.; Lindahl, E. Gromacs: High Performance Molecular Simulations through Multi-Level Parallelism from Laptops to Supercomputers. *SoftwareX* **2015**, *1−2*, 19−25.
(77) Tribello, G. A.; Bonomi, M.; Branduardi, D.; Camilloni, C.; Bussi, G. PLUMED 2: New Feathers for an Old Bird. *Comput. Phys. Commun.* **2014**, *185*, 604−613.
(78) Bussi, G.; Donadio, D.; Parrinello, M. Canonical Sampling through Velocity Rescaling. *J. Chem. Phys.* **2007**, *126*, 014101.
(79) Berendsen, H. J. C.; Postma, J. P. M.; Van Gunsteren, W. F.; Dinola, A.; Haak, J. R. Molecular Dynamics with Coupling to an External Bath. *J. Chem. Phys.* **1984**, *81*, 3684−3690.
(80) Hess, B.; Bekker, H.; Berendsen, H. J. C.; Fraaije, J. G. E. M. LINCS: A Linear Constraint Solver for Molecular Simulations. *J. Comput. Chem.* **1997**, *18*, 1463−1472.

DOI: 10.1021/acs.langmuir.8b01392
Langmuir 2019, 35, 5911−5920

(81) Raiteri, P.; Laio, A.; Gervasio, F. L.; Micheletti, C.; Parrinello, M. Efficient Reconstruction of Complex Free Energy Landscapes by Multiple Walkers Metadynamics. *J. Phys. Chem. B* **2006**, *110*, 3533−3539.
(82) Sano, K.-I.; Shiba, K. A Hexapeptide Motif That Electrostatically Binds to the Surface of Titanium. *J. Am. Chem. Soc.* **2003**, *125*, 14234−14235.
(83) Hayashi, T.; Sano, K.-I.; Shiba, K.; Kumashiro, Y.; Iwahori, K.; Yamashita, I.; Hara, M. Mechanism Underlying Specificity of Proteins Targeting Inorganic Materials. *Nano Lett.* **2006**, *6*, 515−519.
(84) Desmond, J. L.; Juhl, K.; Hassenkam, T.; Stipp, S. L. S.; Walsh, T. R.; Rodger, P. M. Organic-Silica Interactions in Saline: Elucidating the Structural Influence of Calcium in Low-Salinity Enhanced Oil Recovery. *Sci. Rep.* **2017**, *7*, 10944.
(85) Lechner, C. C.; Becker, C. F. W. A Sequence-Function Analysis of the Silica Precipitating Silaffin R5 Peptide. *J. Pept. Sci.* **2014**, *20*, 152−158.
(86) Mitternacht, S.; Schnabel, S.; Bachmann, M.; Janke, W.; Irbäck, A. Differences in Solution Behavior among Four Semiconductor-Binding Peptides. *J. Phys. Chem. B* **2007**, *111*, 4355−4360.

DOI: 10.1021/acs.langmuir.8b01392
Langmuir 2019, 35, 5911−5920